Igneous structure and texture of the ~1.3 Ga Hosenbein anorthosite pluton (Nain, Labrador) and implications for the crystallization of massif-type anorthosite

Ronald Voordouw[1]

Department of Earth Sciences, Memorial University of Newfoundland, St. John's, Newfoundland and Labrador, A1B 3X5, Canada
1. Present address: Council for Geoscience, PO box 900, Pietermaritzburg, South Africa, 3200 <ron.voordouw@gmail.com>

Date received: 05 August 2009 ¶ *Date accepted: 04 February 2010*

ABSTRACT

The ca. 1315 Ma Hosenbein massif-type anorthosite pluton (Nain, Labrador) shows complete exposure of a vertical section, described here for the first time, comprising a ~2000 m-thick Main Zone bound by a ~200 m-thick Marginal Zone. The pluton as a whole consists mostly of monocumulate leucogabbronorite, leuconorite, and anorthosite (~94 vol% of all rocks) with elevated abundances of gabbronorite–ferrodiorite (~27 vol%) in the Marginal Zone. Parental magma likely comprised a plagioclase-phyric basaltic melt, containing ~15–45 vol% plagioclase phenocrysts. Crystallization of this magma produced predominantly massive adcumulate–mesocumulate with less abundant, but regular, occurrences of (in order of relative abundance) gabbronorite–ferrodiorite segregations, mottled texture, foliation, pyroxenite aggregates, and modal layering. Additional key petrographic and compositional features include high-T deformation microstructures in plagioclase, vertically consistent mineral compositions, and enrichment of Fe-Ti-P-HFSE-REE in ferrodiorite. Parts of the Marginal Zone show gneissic–mylonitic fabrics that developed parallel to magma conduits. Collectively these features suggest that the textural and structural evolution of the pluton was controlled by: (a) emplacement of plagioclase-phyric magma, (b) establishment of vast cumulus crystal frameworks, (c) porous flow of intercumulus melt, (d) compaction, and (e) synplutonic deformation. These interpretations contrast with previous work emphasizing the importance of magmatic flow and crystal settling/flotation.

RÉSUMÉ

Un pan vertical des roches d'anorthosite plutonique de Hoseinbein de massif dont la formation remonterait à environ 1 315 Ma (de Nain, au Labrador) semble entièrement exposé et il est décrit ici pour la première fois. Il s'agit en l'occurrence d'une zone principale de plus ou moins 2 000 m d'épaisseur, ceinturée par une zone marginale de plus ou moins 200 m d'épaisseur. Dans son ensemble, la roche plutonique observée se compose principalement de monocumulat de leucogabbronorite, de leuconorite et d'anorthosite (~94% vol. de toutes les roches), dont notamment des quantités élevées de gabbronorite–jotunite (~27% vol.) dans la zone marginale. Le magma parent se composerait vraisemblablement d'un magma de basalte à phénocristaux de plagioclase, contenant approximativement entre 15 et 45% vol. de phénocristaux de plagioclase. La cristallisation de ce magma a produit surtout de l'adcumulat et du mésocumulat massifs, ainsi que des minéralisations régulières mais moins abondantes issues (dans leur ordre d'abondance) de ségrégations de gabbronorite–jotunite, d'une texture marbrée, d'une foliation, d'agrégats pyroxénitiques et de rubanements modaux. Parmi les autres caractéristiques pétrographiques et de composition importantes, il y a des microstructures de déformation de plagioclase survenue à température élevée, des formations minérales uniformes au plan vertical ainsi qu'un enrichissement de Fe-Ti-P-HFS-REE dans la jotunite. Des sections de la zone marginale présentent des traces d'une texture gneissique-mylonitique qui s'est formée parallèlement aux canalisations magmatiques. Dans l'ensemble, ces caractéristiques portent à croire que l'évolution de la texture et de la structure des roches plutoniques a été déterminée par les phénomènes suivants: (a) l'emplacement du magma de phénocristaux de plagioclase; (b) l'établissement de vastes complexes de cristaux de cumulus; (c) l'écoulement poreux de magma intercumulus; (d) le compactage; et (e) une déformation synplutonique. Ces interprétations diffèrent quelque peu des travaux précédents, où l'accent avait été mis sur l'importance de l'écoulement magmatique, et la décantation et la flottation de cristaux.

[Traduit par la redaction]

0843-5561|08|00019–17$3.55|0
doi: 10.4138/atlgeol.2010.003

INTRODUCTION

Proterozoic massif-type anorthosite is one of six anorthosite types (Ashwal 1993), which also include anorthosite in layered mafic intrusions (e.g., Bushveld Complex) and lunar anorthosite. Based on its high proportion (~70–100 vol%) of intermediate plagioclase ($An_{40–60}$) and lack of complementary mafic–ultramafic cumulates, it is inferred that magmas parental to massif-type anorthosite originated from the fractional crystallization and contamination of basaltic magma in the crust–mantle boundary zone (Duchesne 1984; Ashwal 1993; Emslie *et al*. 1994). The plagioclase-phyric basaltic magmas that developed through fractionation and contamination were then remobilized to form massif-type anorthosite intrusions at mid- to upper-levels in the continental crust (Duchesne 1984; Ashwal 1993; Emslie *et al*. 1994).

The petrogenetic model for massif-type anorthosite differs from the more *in situ* origins postulated for other types of anorthosite (Fig. 1). Lens-like bodies of Archaean megacrystic anorthosite (e.g., Fiskenæsset, Bad Vermillion Lake), for example, likely formed through flotation of plagioclase phenocrysts during *in situ* fractional crystallization of basaltic parental magma (Windley *et al*. 1973; Ashwal *et al*. 1983). Anorthosite layers in layered intrusions and ocean basins are modeled in similar ways (e.g., Kruger and Marsh 1985; Eales *et al*. 1986). The vast expanses of lunar anorthosite also formed through the flotation of plagioclase crystals in the same basaltic magma from which it crystallized (Longhi 1978; Walker 1983; Ashwal 1993).

In decades preceding the idea that plagioclase accumulation and crystallization could occur at separate places in the lithosphere, petrogenetic models for massif-type anorthosite favoured an *in situ* origin similar to those currently accepted for layered intrusive (and other) anorthosite. These earlier models were built on the assumption that "significant mafic to ultramafic material was buried beneath anorthosite massifs" (Ashwal 1993, p. 205), which has since widely been disproved (Ashwal 1993; Funck *et al*. 2000). Regardless, the *in situ* models influenced early work on massif-type anorthosite from the Nain area (Labrador), with field investigations widely reporting igneous textures and structures consistent with magma undergoing vigorous magmatic convection and fractional crystallization (Morse 1969a, 1972; Berg 1972, 1973; Davies 1973; Ranson 1975, 1981). Since then, no attempt has been made to integrate the field characteristics with the newer petrogenetic models for massif-type anorthosite, leaving some uncertainty in regards to how viscous plagioclase-phyric parental magmas could have crystallized under apparently dynamic conditions.

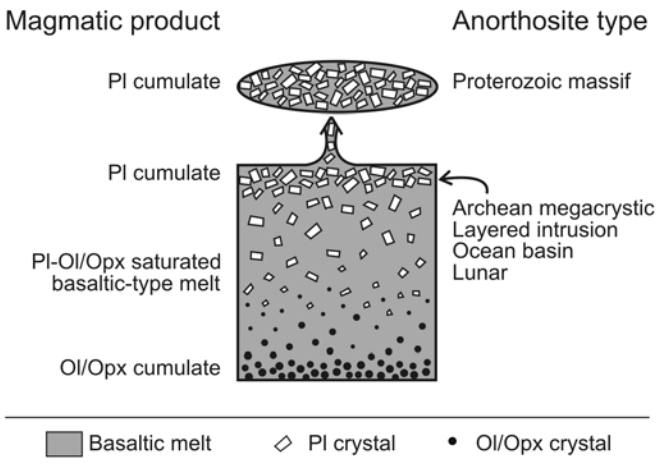

Fig. 1. Schematic model showing the differences between petrogenesis of Proterozoic massif-type and other types of anorthosite (Archean megacrystic, layered intrusion, ocean basin, lunar). Abbreviations; Pl = plagioclase, Ol = olivine, Opx = orthopyroxene.

This article attempts to resolve the contrast between early field studies on Nain anorthosite and currently accepted petrogenetic models through detailed mapping of the Hosenbein pluton. This intrusion was traversed to collect data on the relative abundances of igneous rock types, textures, and structures, which were then used to construct the first complete vertical section through an anorthosite pluton in the Nain batholith and to discuss the relative significance of magmatic processes involved in its textural and structural evolution (Voordouw 2006). Those data are presented in this paper.

Geological Setting

The Hosenbein pluton lies near the center of the 1364–1289 Ma Nain anorthosite-granite batholith (Fig. 2a), which is arguably the world's type locality for massif-type anorthosite. The Nain batholith was emplaced across the intersection between crustal-scale structures related to the east–west trending Gardar-Voisey's Bay Fault Zone and the north–south trending Paleoproterozoic Torngat Orogen (Myers *et al*. 2008). Together, these structures likely controlled the ascent and emplacement of magmas (Myers *et al*. 2008) and formation of the world-class Voisey's Bay Ni-Cu deposit (Evans-Lamswood *et al*. 2000).

The Nain batholith was emplaced in two magmatic episodes (Myers *et al*. 2008), each of which began with emplacement of massif-type anorthosite (1364–1340 Ma and 1319–1295 Ma) and ended with granitoids (1322–1319 Ma and 1292–1289 Ma). Anorthosite is synonymous with a range of plagioclase cumulates that include anorthosite *sensu stricto* (≥90 vol % plagioclase) as well as leuconorite, leucotroctolite and leucogabbronorite (each containing 67.5–90 vol% plagioclase). Granitoids consist mostly of granite, quartz monzonite and monzonite, which range from biotite- and hornblende-bearing to pyroxene- and olivine-bearing (Emslie and Stirling 1993). Troctolitic and gabbronoritic magmas (e.g., Kiglapait in Morse 1969b) were emplaced in both episodes (Myers *et al*. 2008), sometimes in close association with ferrodiorite and monzonite (de Waard *et al*. 1976; Gaskill 2005).

The Hosenbein pluton (Figs 2b, 2c) lies near the center of the Nain batholith and was emplaced at ca. 1315 Ma (Voordouw 2006), near the beginning of episode 2. Parts of this pluton were mapped over the last few decades (Wheeler

1960; Rubins and de Waard 1971; Rubins 1973; Ryan 2000, 2001) with the current boundaries identified through mapping as part of a thesis study by the author (Voordouw 2006). The structural subdivisions, textures, and structures of this pluton are described in more detail below.

Methodology

Geological mapping of the Hosenbein pluton was done at 1:10 000 to improve on 1:50 000 maps published by the Geological Survey of Newfoundland and Labrador (Ryan 2000,

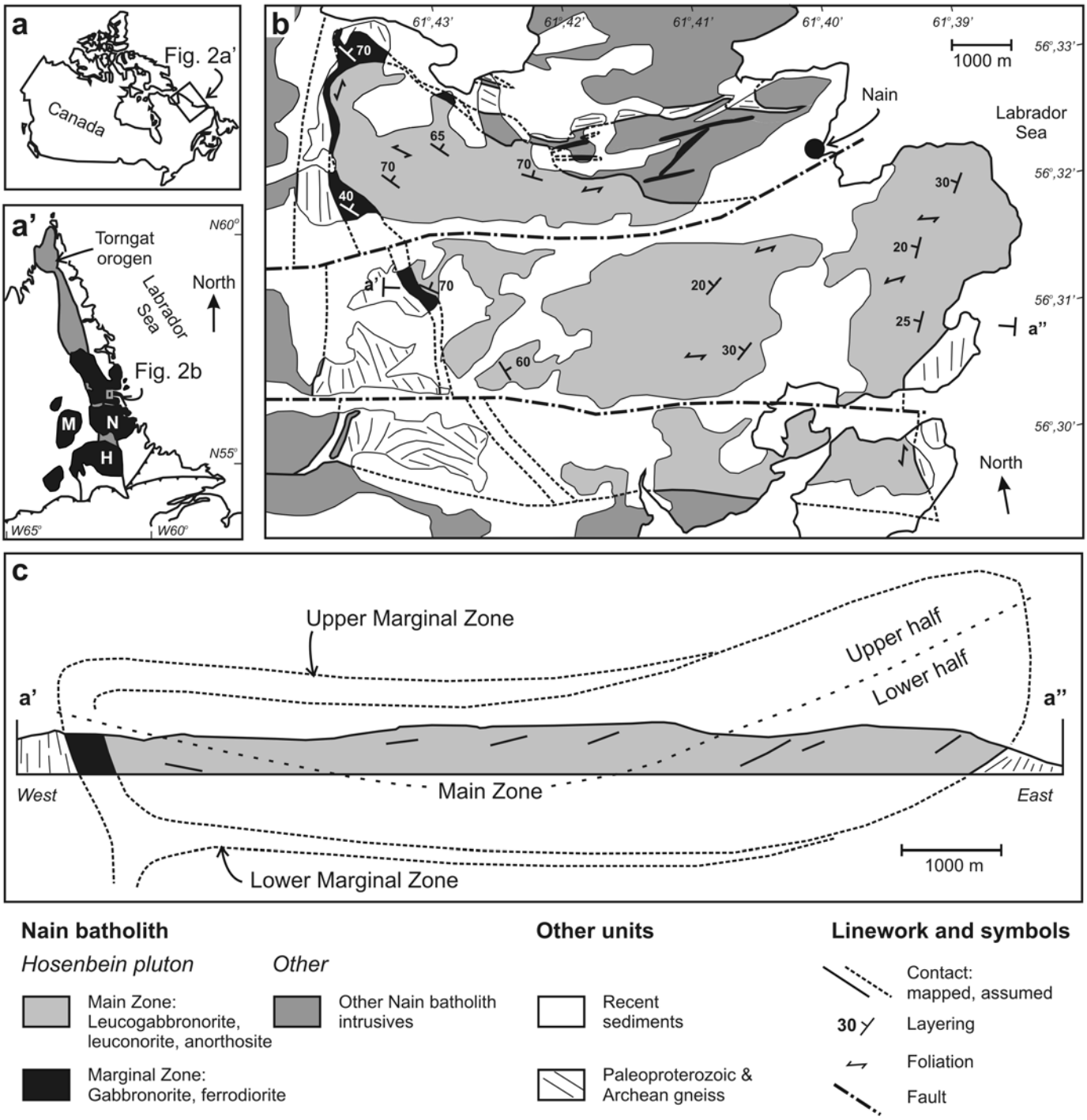

Fig. 2. (a) Locality maps of the study area in Canada and (a') northern Labrador, the latter showing several large Mesoproterozoic anorthosite-granite batholiths as well as the Torngat Orogen. Batholiths are: N = Nain, M = Mistasin, H = Harp Lake. (b) Geological map of the Hosenbein pluton. (c) East–west cross-section through the Hosenbein pluton with a dotted line delineating the lower and upper halves. Cross-section line a'–a" is shown in Fig. 2b.

2001). Exposures are abundant and were mapped through ~200 km of foot traverses that included recording detailed descriptions at 441 point locations. The vertical distribution of rock types, textures, and structures was determined by subdividing the lower and upper halves of the Main Zone into five intervals each (Fig. 3), with each containing between 31–54 point locations.

Quantitative mineralogical and geochemical data were determined at Memorial University of Newfoundland. Mineral compositions for plagioclase (N = 93), clinopyroxene (N = 65) and orthopyroxene (N = 48) cores were obtained with a Cameca SX-50 microprobe, using wavelength-dispersive spectrometry (WDS) with count times between ~10–20 seconds. Whole-rock major element abundances for anorthosite–leucogabbronorite (N = 5) and gabbronorite–ferrodiorite (N = 3) were determined by X-ray fluorescence on a Fissions/Applies Research Laboratories model 8420+ sequential WD X-ray spectrometer, using the operating conditions described by Longerich (1995). Trace and rare earth elements were determined with a Finnigan Neptune multicollector ICP-MS following the procedures of Longerich *et al*. (1990).

RESULTS

New geological mapping outlines the Hosenbein pluton as a T-shaped basinal structure subdivided into Main and Marginal zones (Fig. 2b, 2c). The Main Zone (~50 km²) is ~2000 m thick and is bound by the Marginal Zone (~2 km²), which is an average of ~200 m thick. The Marginal Zone is further subdivided into Lower and Upper units that bound the lower half and upper halves of the Main Zone, respectively (Fig. 2c). The northern and western contacts of the pluton abut Paleoproterozoic(?) ultramafic–mafic gneiss or dips gently underneath the ca. 1340 Ma Unity massif-type anorthosite (Voordouw 2006). The southern part of the pluton is crosscut by the ca. 1310 Ma Kikkertavak anorthosite complex, and the eastern contact abuts Paleoproterozoic(?) anorthosite gneiss or lies underwater.

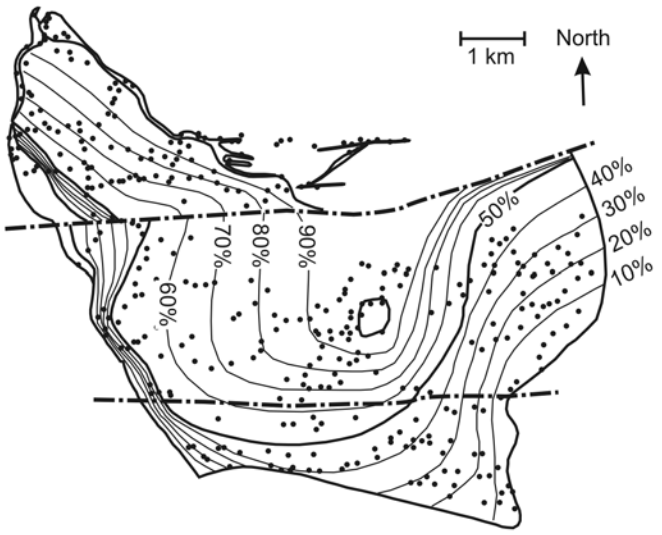

Fig. 3. Sketch map of the Hosenbein pluton showing described point locations (dots) and subdivision of the Main Zone into 10 intervals, referred to as % vertical extent through the Main Zone.

The Marginal and Main Zones are described below in stratigraphic succession from bottom to top. The emphasis is on lithologies, texture, and structure, although some supplemental petrographic, mineralogical, and geochemical data are also provided.

Lower Marginal Zone

The Lower Marginal Zone is a composite subunit formed by partial ring dykes, straight dykes, and lenticular sheets. Rock types consist of medium- to very coarse-grained leucogabbronorite (~65 vol%), gabbronorite–ferrodiorite (~30 vol%), and anorthosite (~5 vol%). Intra-subunit contacts range from gradational to sharp, with the latter lacking chilled margins, and inclusions of any lithology can occur in the others. Contacts with the overlying Main Zone are gradational whereas those with underlying Paleoproterozoic(?) gneiss are sharp.

Textures and structures are diverse and include massive, mottled, modally layered, and foliated rocks. Massive and mottled rocks may show adcumulate (~93–100% cumulus phase), mesocumulate (~85–93%), or orthocumulate (~75–85%) texture, with mottled rocks comprising two or more textures in close association (cm- to m-scale). Modal layering occurs at ~25% of localities and is defined by sharp to gradational changes in the modal proportions of plagioclase and pyroxene, over widths ranging from just ~1 cm to ~10 m. Most layers are moderately dipping to subvertical (~40°–90°) and strike parallel to the north–south trending Paleoproterozoic(?) gneiss that underlies it. Textures are typically recrystallised and granoblastic ("gneissic"), rather than primary igneous (Figs 4a, 4b), and grade into steeply dipping and finely layered rocks comprising relict igneous crystals in an even finer grained granoblastic groundmass ("mylonitic"). Foliation occurs at ~15% of localities and is defined by the shape preferred orientation (SPO) of cumulus crystals or crystal aggregates of pyroxene and/or plagioclase, with the latter defining foliation in layered gneissic–mylonitic rocks. Foliations strike parallel to modal layering and Paleoproterozoic(?) structures.

Inclusions were found at ~10% of localities, and include both autoliths and xenoliths. Autoliths consist of any Marginal Zone lithology hosted within a younger Marginal Zone lithology whereas xenoliths consist of Paleoproterozoic(?) gneiss and pervasively recrystallised, ca. 1340, Unity and Mount Lister anorthosites. Many autoliths and xenoliths have tablet-like forms that lie parallel to modal layering, foliation and nearby Paleoproterozoic (?) structures. Pegmatoids form lens-like bodies that consist of coarse- to very coarse-grained leucogabbronorite, gabbronorite, or ferrodiorite, some of which have

crescumulate texture. Like the inclusions, pegmatoids strike parallel to most of the other planar features in their vicinity.

Modal mineralogies are defined by plagioclase (~30–95 vol%), orthopyroxene (<1–45 vol%) and clinopyroxene (<1–25 vol%), with accessory (<10 vol%) abundances of Fe-Ti oxide, olivine, hornblende, biotite, apatite, and secondary minerals (e.g., sericite, uralite, chlorite, carbonate). Plagioclase, olivine and, in places, orthopyroxene are the only cumulus minerals. Compositions range from ~$An_{50–60}$ for plagioclase, ~$En_{55–59}$ for orthopyroxene and ~$En_{36–40}$ for clinopyroxene, and average ~Fo_{45} for olivine (Voordouw 2006).

Main Zone

The Main Zone consists mostly of medium- to coarse-grained leucogabbronorite–leuconorite (~60 vol%) and anorthosite (~40%) with <1 vol% gabbronorite–ferrodiorite. Abundances of leucogabbronorite–leuconorite are especially high, between ~60–80% of the vertical extent through the Main Zone, whereas anorthosite is abundant in the lower half (Fig. 5). The gradational contact with the Marginal Zone is marked by an increase in pyroxene and in the dip of modal layering. The northeastern ~20 km² of the Main Zone consists of block structure developed directly underneath the Unity anorthosite (Fig. 6), with block structure comprising numerous xenoliths (up to ~100 m long) of pervasively recrystallised Unity anorthosite hosted by igneous-textured leucogabbronorite–leuconorite (Fig. 7a).

Leucogabbronorite–leuconorite and anorthosite are mostly massive with less abundant mottled rocks (~20% of localities). Massive anorthosite has adcumulate texture comprising tightly packed cumulus plagioclase with accessory (<10 vol%) abundances of intercumulus pyroxene and Fe-Ti oxide. The mesocumulate texture that characterizes leucogabbronorite–leuconorite is defined by higher proportions of intercumulus pyroxene and Fe-Ti oxide. Most massive rocks, however, show

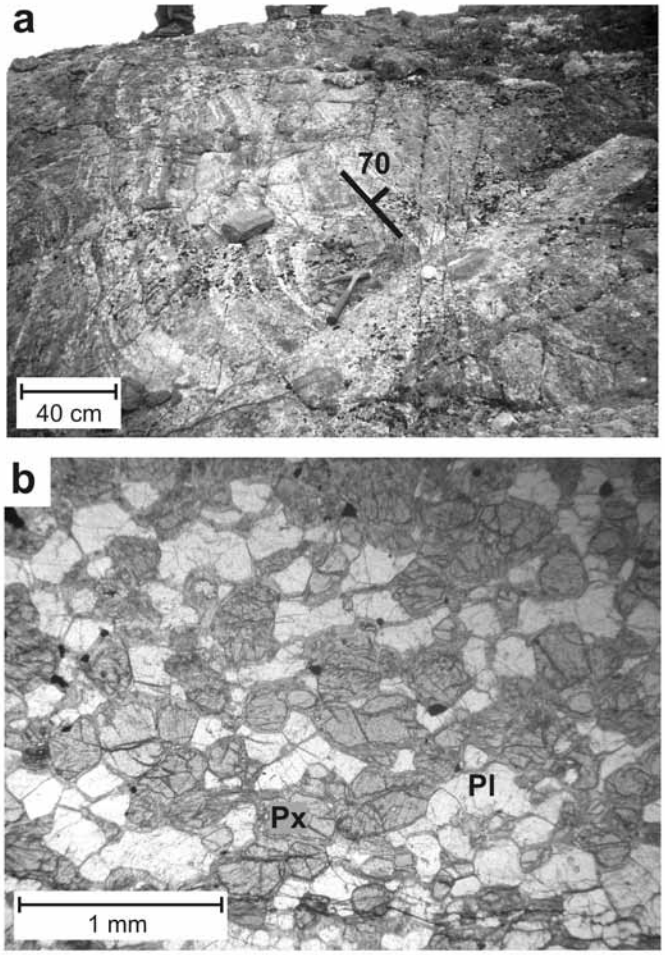

Fig. 4. (a) Outcrop photograph of gneissic layering between gabbronorite, leucogabbronorite and anorthosite in the Lower Marginal Zone, ~6.5 km west-southwest of Nain. Strike and dip symbol shows orientation of layers. (b) Photomicrograph of granoblastic gabbronorite from the Lower Marginal Zone (Pl = plagioclase, Px = pyroxene).

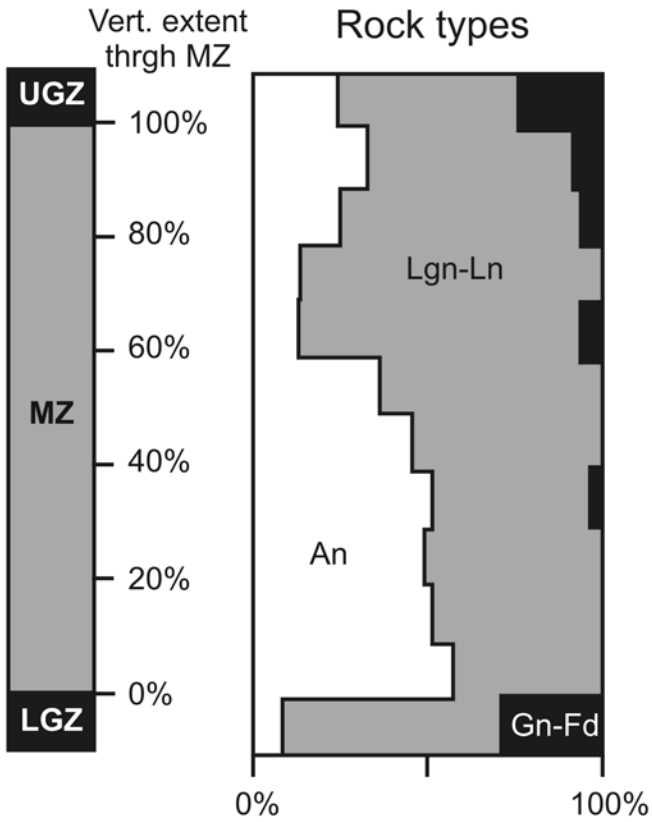

Fig. 5. Relative abundances of anorthosite (An), leucogabbronorite–leuconorite (Lgn–Ln) and gabbronorite–ferrodiorite (Gn–Fd) in the Lower Marginal (LGZ), Main (MZ) and Upper Marginal (UGZ) zones. Abundances in the Main Zone are expressed in terms of "vertical extent through the Main Zone", where 0% marks the base and 100% the top. This vertical extent is a maximum of ~2000 m.

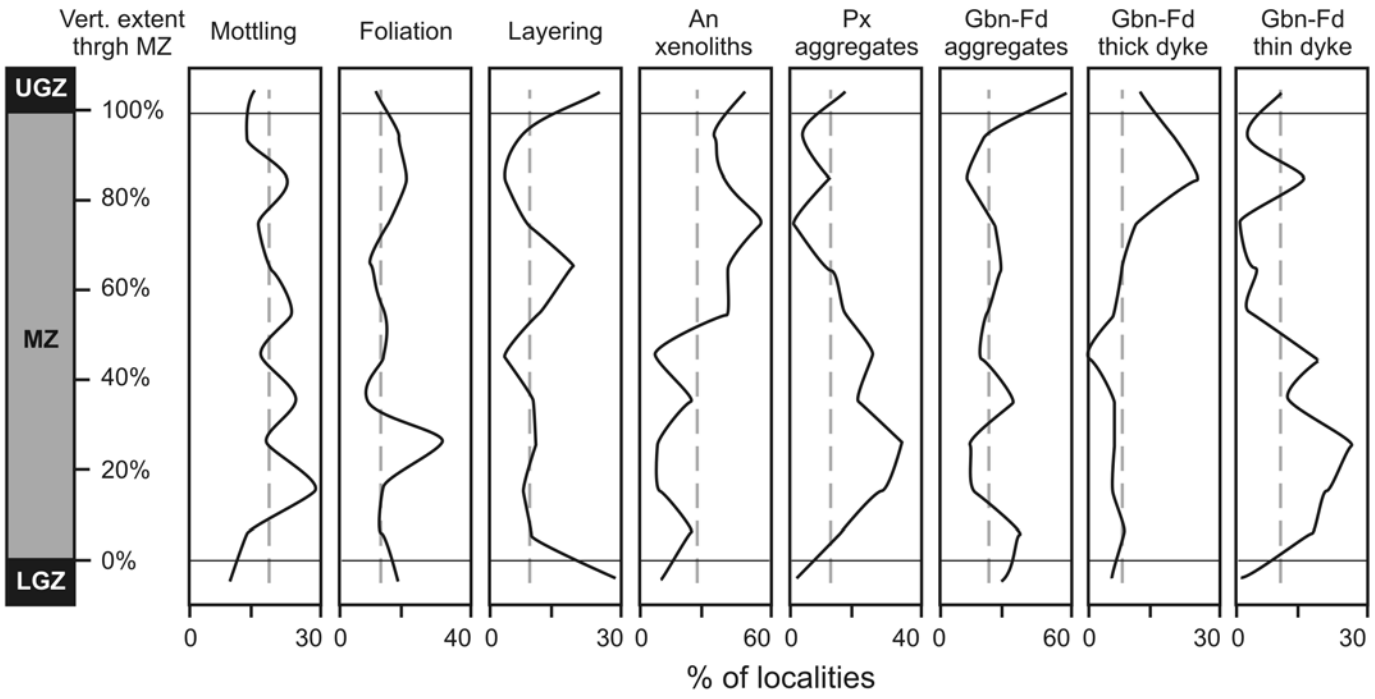

Fig. 6. Vertical distribution of igneous textures and structures in the Marginal and Main Zones. See text for more description. Abbreviations; An = anorthosite, Px = pyroxene, Gbn–Fd = gabbronorite–ferrodiorite. Pluton subunit abbreviations are the same as Fig. 5.

a subtle interspersing of adcumulate and mesocumulate textures (Fig. 7b) that in some cases grades into more coarsely segregated mottled rocks (Fig. 7c). These mottled rocks consist of subspherical to shapeless patches (~1–1000 cm in size) of mesocumulate leucogabbronorite–leuconorite hosted in adcumulate anorthosite. Intercumulus pyroxene may show optical continuity across a single patch, although this situation appears to be rare. Other mottles approach gabbronorite–ferrodiorite composition and may further aggregate into large patches and dykes, as described in more detail below. In both massive and mottled rocks, cumulus plagioclase crystals impinge on at least one, and typically more, neighbouring plagioclase crystals.

Foliated leucogabbronorite–leuconorite and anorthosite occur at ~15% of localities, showing mostly uniform distribution except for an anomalously high concentration at ~20–30% of the vertical extent through the Main Zone (Fig. 6). Foliation is defined by disc-shaped intercumulus crystals of pyroxene and/or Fe-Ti oxide (Fig. 7d), and generally strikes east–west and dips moderately to steeply north (~30°–90°).

Modally layered rocks composed of leucogabbronorite–leuconorite and anorthosite occur at just 5% of localities, and are therefore significantly less abundant than massive, mottled, and foliated rocks. At ~60–70% of the vertical extent through the Main Zone, however, modal layering occurs at an anomalously high proportion (~15%) of localities (Fig. 6). Typical layers comprise lens-like bodies of mesocumulate leucogabbronorite–leuconorite hosted in adcumulate anorthosite (Fig. 7e). These lenses are typically less than a meter thick and tens of meters long, and dip at gentle to moderate angles towards the center of the pluton.

Intercumulus aggregates of relatively large pyroxene crystals occur at ~15% of localities in the Main Zone and are especially abundant in the lower half (Fig. 6). They are of three types: (1) vein-like, (2) pod-like, and (3) corona-like. Vein-like aggregates comprise steeply dipping layers that are typically a few centimetres thick and up to tens of meters long (Fig. 8a). Their orientation with respect to foliation and modal layering ranges from concordant to highly discordant. Pod-like aggregates are shorter and rounder, and may consist of just a few, exceptionally large, pyroxene crystals. Corona-like aggregates are formed at contacts with Unity anorthosite xenoliths (Fig. 8b) and synplutonic gabbronorite–ferrodiorite dykes, with sizes ranging from ~1–2 cm centimetres thick and ~10–100 cm long.

Gabbronorite–ferrodiorite forms dykes (up to ~10 m thick) and shapeless aggregates (up to ~500 m^2) throughout the Main Zone, occurring at a remarkable ~35% of localities. Thicker (>30 cm) dykes are particularly abundant within the uppermost parts of the Main Zone whereas the lower half contains more thin (<1 cm) dykes (Fig. 6). Contacts with host rocks range from curved and gradational to sharp and planar (Fig. 7f), and typically lack chilled margins. Textures range from orthocumulate to granular, with some granular-textured dykes showing pervasive foliation and modal layering striking parallel to the walls.

Modal mineralogies of lithologies in the Main Zone typically consist of plagioclase (40–100 vol%), orthopyroxene (0–30 vol%), and clinopyroxene (0–15 vol%), with accessory abun-

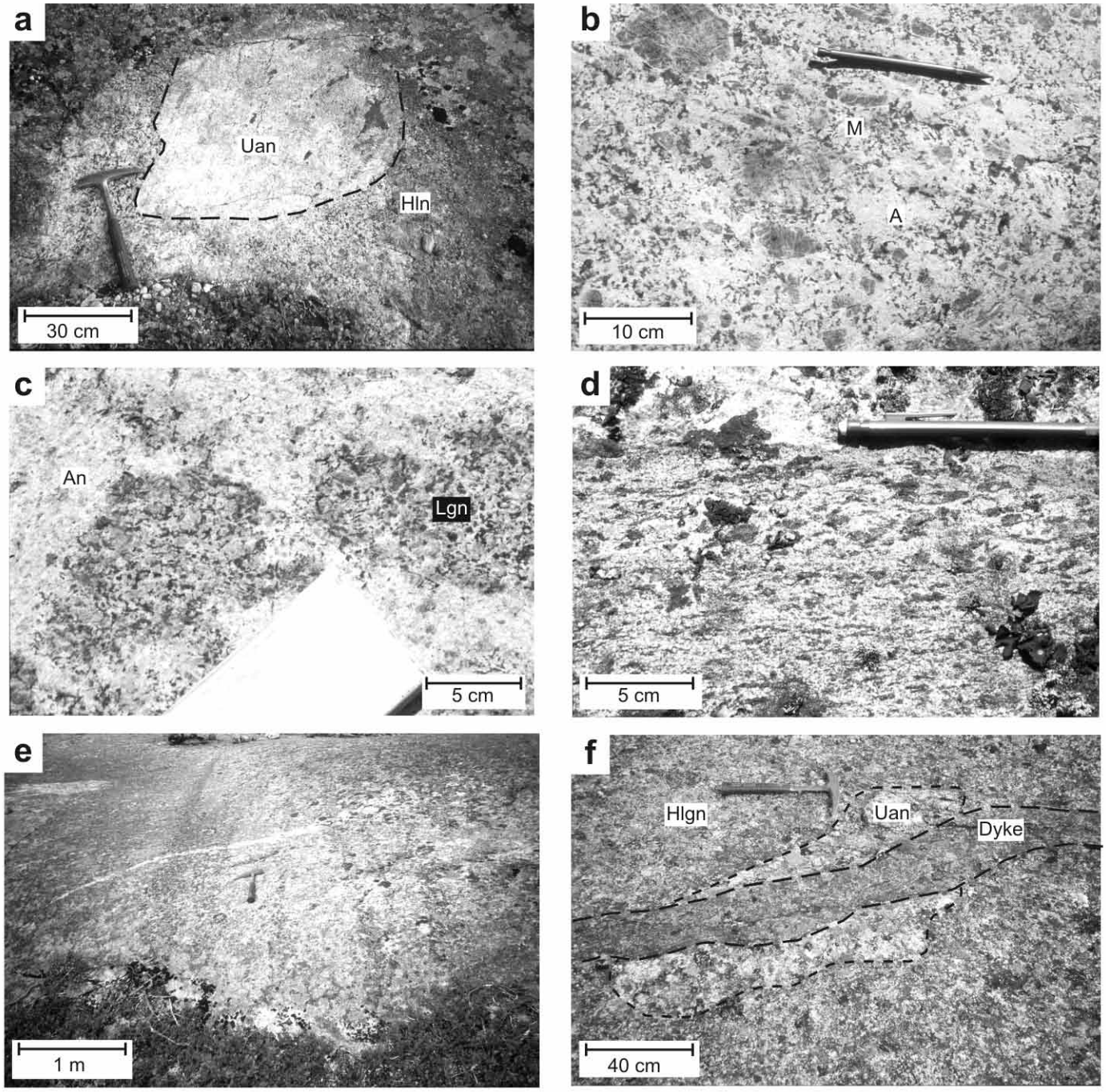

Fig. 7. Outcrop photographs showing igneous textures and structures in the Main Zone. (a) Xenolith of recrystallized Unity anorthosite (Uan) within mesocumulate Hosenbein leuconorite (Hln), ~5 km southwest of Nain. (b) Subtle interspersing of (A) adcumulate and (M) mesocumulate textures in massive leucogabbronorite, ~1.5 km south of Nain. (c) Mottled texture defined by subspherical aggregates of mesocumulate leucogabbronorite (Lgn) within adcumulate anorthosite (An), ~2.5 km south of Nain. (d) Leuconorite with foliated intercumulus pyroxene, ~5 km south of Nain. Pen lies parallel to foliation. (e) Modal layering between anorthosite and leucogabbronorite ~5 km west of Nain. (f) Ferrodiorite dyke cutting across Hosenbein leucogabbronorite (Hlgn) and a xenolith of Unity anorthosite (Uan), also ~5 km west of Nain. The contact across the xenolith is sharp whereas it is more gradational with leucogabbronorite.

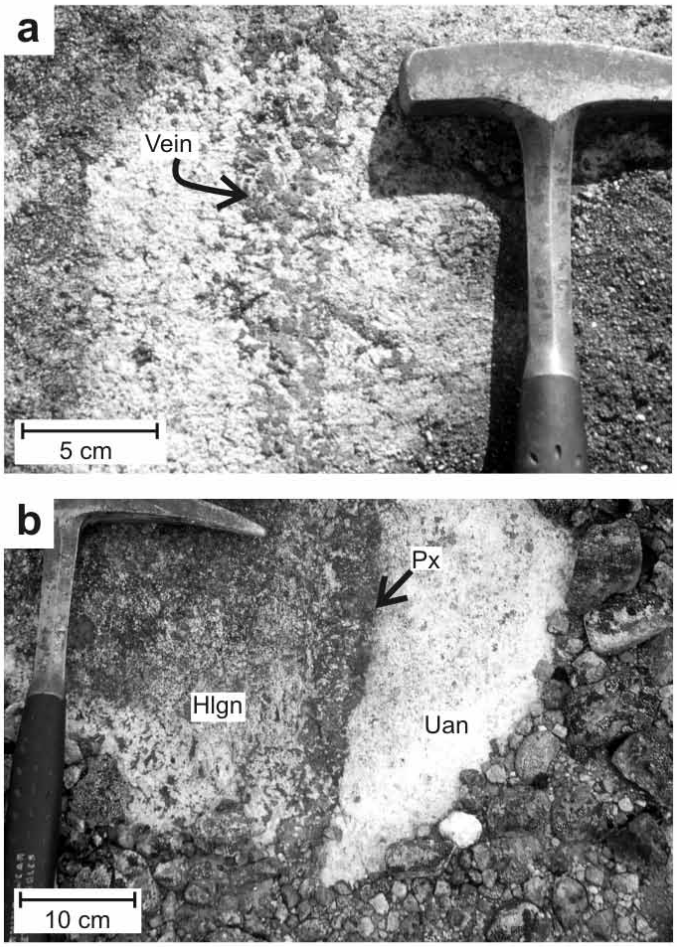

Fig. 8. Outcrop photographs showing pyroxenite aggregates within the Main Zone. (a) Vein-like aggregate within adcumulate anorthosite, ~4 km west of Nain. (b) Corona-like aggregate at a contact between Hosenbein anorthosite (Hlgn) and a xenolith of Unity anorthosite (Han), ~3 km west-southwest of Nain. See text for more detail.

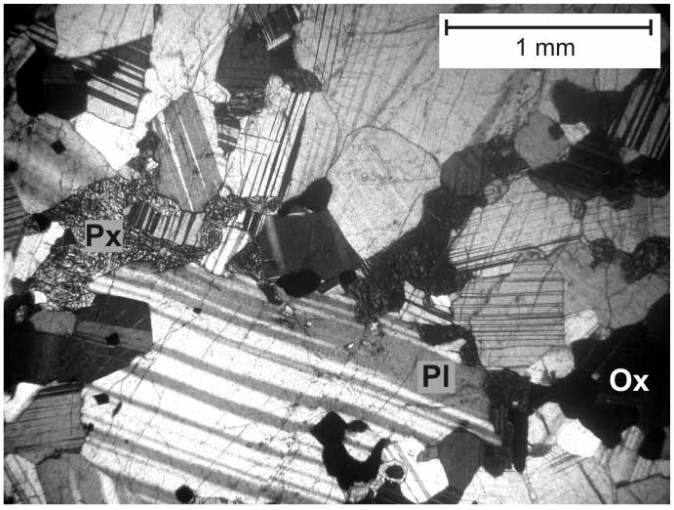

Fig. 9. Photomicrograph of Main Zone leucogabbronorite showing plagioclase (Pl) crystals with deformation twins, impinging margins and brittle fractures, as well as intercumulus pyroxene (Px) and Fe-Ti oxide (Ox).

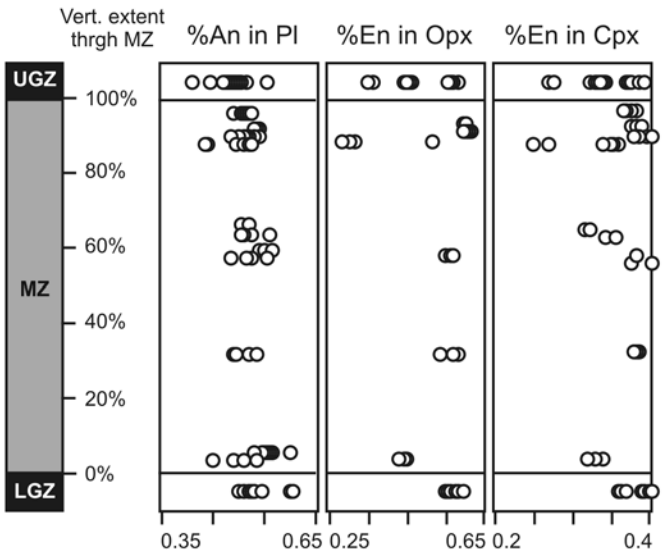

Fig. 10. Vertical distribution of plagioclase (Pl), orthopyroxene (Opx) and clinopyroxene (Cpx) compositions across the Marginal and Main Zones. Compositions are expressed in terms of mol% anorthite (An) and enstatite (En). Subunit abbreviations are the same as Fig. 5.

dances of Fe-Ti oxide, sericite, uralite, apatite, hornblende, biotite, chlorite, carbonate, epidote, and quartz. Cumulus plagioclase crystals universally impinge on their neighbours (Fig. 9), and many have deformation twins, serrated margins, undulatory extinction, and/or brittle fractures. Core compositions range between $An_{43–60}$, but are vertically uniform (Fig. 10), and compositional zoning consists only of narrow Ca-rich rims (Voordouw 2006). Orthopyroxene and clinopyroxene are intercumulus and have compositions ranging from $En_{28–62}$ and $En_{25–40}$, respectively. Besides the occurrence of the most Fe-rich pyroxene within the uppermost part of the Main Zone, there appears to be no systematic vertical change in pyroxene composition.

Whole-rock major-oxide abundances in leucogabbronorite–leuconorite include high amounts of Al_2O_3, Na_2O, Ba, and Sr (Table 1), consistent with high abundances of plagioclase. FeO shows strong positive correlations ($r \geq 0.9$) with MnO, MgO, Y, Zr, Ta, U, and rare earth elements (REE). Spidergrams show depletions in high field strength elements (HFSE) (Fig. 11) and REE patterns show a positive Eu anomaly as well as enrichment of light REE relative to heavy REE. Gabbronorite shows relatively high wt% MgO, spidergrams that are similar to enriched leucogabbronorite–leuconorite (Fig. 11), and flat REE patterns. Ferrodiorite contains high wt% TiO_2, FeO, P_2O_5, HFSE, and REE.

Table 1. Major (wt%), trace and rare earth (ppm) element data for leucogabbronorite–leuconorite (Lgn–Ln), gabbronorite (Gn) and ferrodiorite (Fd) from the Main Zone (MZ), Lower Marginal Zone (LGZ) and Upper Marginal Zone (UGZ).

Sample	01-24-14	01-21-30	00-2-4	00-22-11	01-33-31	00-25-9d	01-28-5b	01-34-1
Subunit	MZ	MZ	MZ	MZ	LGZ	LGZ	UGZ	UGZ
Lithology	Lgn-Ln	Lgn-Ln	Lgn-Ln	Lgn-Ln	Lgn-Ln	Gn	Gn	Fd
SiO_2	51.61	54.10	52.83	52.87	50.89	48.20	48.81	41.75
TiO_2	0.58	0.07	0.29	0.33	1.75	1.11	1.49	4.84
Al_2O_3	23.84	27.54	22.85	21.19	19.68	14.69	15.06	12.10
FeO^t	4.82	0.76	4.59	6.24	8.11	13.27	12.41	17.65
MnO	0.06	0.01	0.07	0.10	0.13	0.20	0.18	0.23
MgO	2.47	0.31	3.52	4.76	3.10	7.02	7.65	6.02
CaO	10.12	10.75	10.31	8.72	9.19	10.01	9.05	10.49
Na_2O	3.79	4.50	3.85	3.39	3.46	2.41	2.44	2.12
K_2O	0.34	0.38	0.35	0.40	0.44	0.09	0.22	0.18
P_2O_5	0.02	0.01	0.01	0.06	0.35	0.01	0.25	2.01
Total	97.65	98.43	98.67	98.06	97.11	97.02	97.56	97.39
Cs		0.05			0.01		0.01	0.00
Rb	1.46	1.71	0.90	2.18	1.41	0.24	1.13	0.82
Ba	414	422	379	372	636	120	281	333
Sr	902	897	720	593	603	178	564	457
Y	3	0	4	4	18	17	9	32
Zr	7	3	11	16	17	31	21	44
Hf	0.337	0.285	0.412	0.847	0.720	1.393	0.784	2.121
Nb	0	0	0	1	11	1	4	7
Cr	93	14	18	84	67	144	87	0
V	97	0	57	60	99	311	275	436
Li	4.79	3.36	10.87	5.34	7.46	5.98	3.46	4.10
Ta	0.08	0.05	0.06	0.10	0.54	0.11	0.23	0.22
Th	0.07	0.02	0.09	2.53	0.22	2.85	0.10	0.40
U	0.02	0.01	0.02	0.03	0.04	0.05	0.03	0.09
Pb	1.58	2.72	1.34	1.53	3.77	1.49	1.76	1.90
Bi	0.01	0.01	0.01	0.00	0.01	0.01	0.01	0.00
Mo	0.12	0.08	0.10	0.20	0.78	0.24	0.29	0.80
La	3.396	4.889	3.394	5.547	18.632	2.664	10.158	32.604
Ce	6	8	7	11	44	7	23	80
Pr	0.746	0.734	0.841	1.303	5.274	1.099	3.052	10.498
Nd	3.035	2.399	3.590	5.366	22.915	6.005	13.143	48.298
Sm	0.570	0.255	0.756	1.004	4.441	1.950	2.529	9.555
Eu	0.885	0.744	0.998	0.978	2.211	0.910	1.113	2.556
Gd	0.519	0.126	0.758	0.959	4.170	2.682	2.311	8.949
Tb	0.075	0.014	0.115	0.142	0.592	0.465	0.313	1.213
Dy	0.453	0.070	0.722	0.867	3.404	3.111	1.898	6.636
Ho	0.090	0.011	0.144	0.179	0.681	0.669	0.363	1.270
Er	0.265	0.034	0.402	0.501	1.818	1.958	0.964	3.218
Tm	0.044	0.011	0.065	0.070	0.249	0.289	0.143	0.406
Yb	0.246	0.020	0.375	0.482	1.524	1.884	0.861	2.355
Lu	0.035	0.000	0.057	0.074	0.229	0.282	0.013	0.329

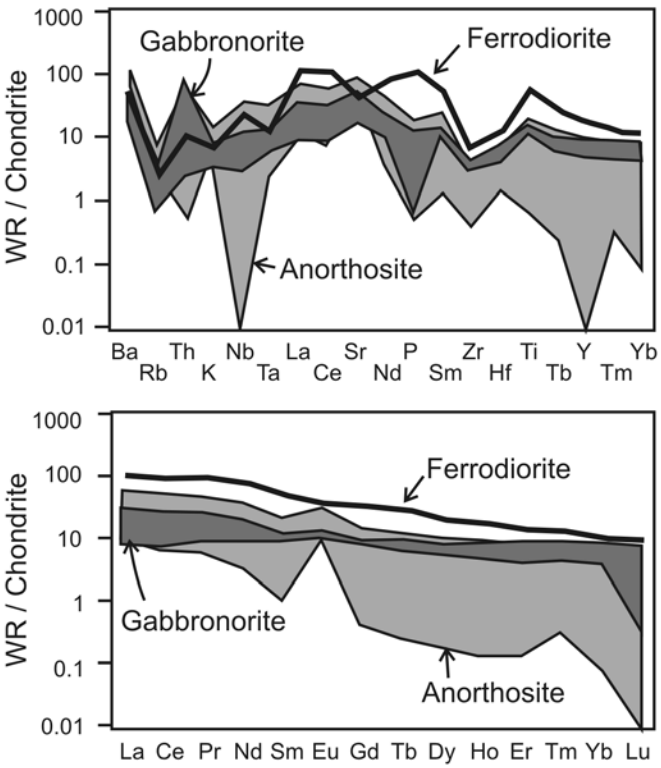

Fig. 11. Chondrite-normalized trace element spidergrams (top) and rare earth element (REE) plots (bottom) for anorthosite–leucogabbronorite–leuconorite (An–Lgn, N = 5), gabbronorite (N = 2) and ferrodiorite (N = 1). Plagioclase cumulates were sampled from the Main Zone (N = 4) and Lower Marginal Zone (N = 1), gabbronorite from Lower and Upper Marginal Zones and ferrodiorite from the Upper Marginal Zone. Normalization values are from Thompson (1982) and Nakamura (1974) with additions from Haskin *et al*. (1968).

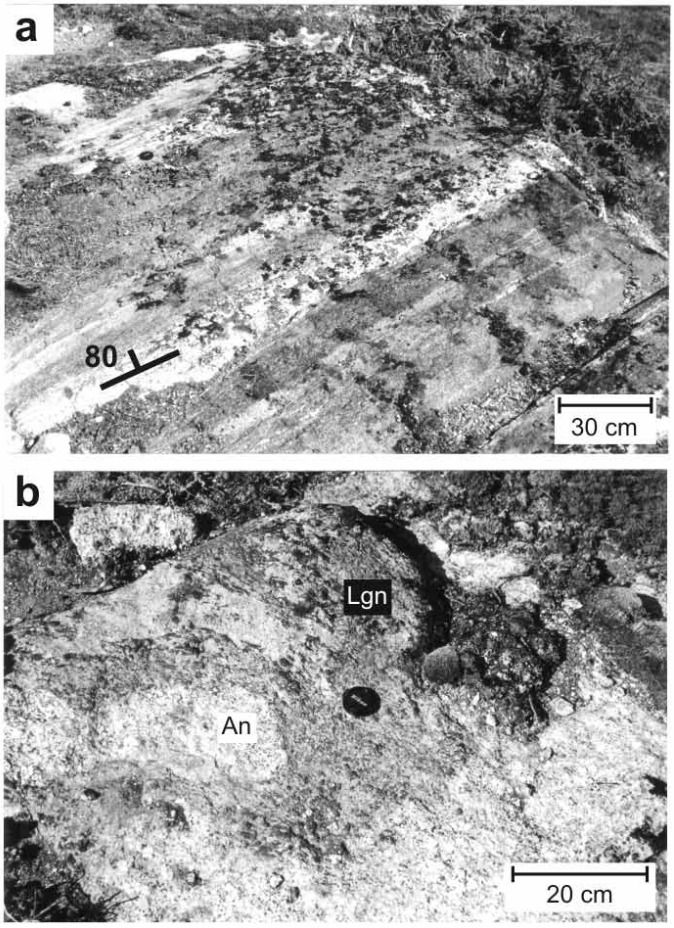

Fig. 12. Outcrop photographs of the Upper Marginal Zone. (a) Gneissic layering between gabbronorite, leucogabbronorite and anorthosite, ~3 km west of Nain. Strike and dip symbol indicates layering orientation. (b) Autoliths of partially disaggregated anorthosite (An) within massive to locally foliated leucogabbronorite (Lgn), ~6 km northeast of Nain.

Upper Marginal Zone

The Upper Marginal Zone is compositionally, structurally and texturally similar to the Lower Marginal Zone, comprising several small sheet-like bodies of medium-grained to very coarse-grained leucogabbronorite (~50 vol%), gabbronorite–ferrodiorite (~25 vol%), and anorthosite (~25 vol%). Contacts between lithologies are likewise sharp to gradational, with some sharp contacts exhibiting an intrusive nature.

Structures and textures are mostly massive, modally layered (25% of localities), mottled (15%), and foliated (10%), with massive and mottled rocks similar to those in the Lower Marginal Zone. Well developed modal layering is typically associated with foliation and equigranular granoblastic (or gneissic) texture (Fig. 12a), just like in the Lower Marginal Zone. Gradations from gneissic to mylonitic layering occur as well. Orientations strike east–west, parallel to the Voisey's Bay-Gardar Fault Zone, and are also moderately dipping to subvertical (~50°–90°). Other igneous structures that strike parallel to this fault zone include foliation and tablet-shaped inclusions.

Inclusions consist of autoliths and xenoliths. Autoliths comprise any type of Upper Marginal Zone lithologies hosted in another type, and attest to the composite nature of this subunit. Contacts between autoliths and host rocks are sharp to gradational, with some gradational contacts formed by mixed zones of disaggregated crystals and host rock (Fig. 12b). Xenoliths include tablets of reworked Paleoproterozoic(?) gneiss that lie parallel to modal layering and foliation.

Modal mineralogies consist of plagioclase (15–95 vol%), orthopyroxene (<1–60 vol%), and clinopyroxene (<1–40 vol%) with accessory abundances of Fe-Ti oxide, hornblende, biotite, apatite and secondary minerals (sericite, uralite, chlorite, car-

bonate). Cumulus minerals consist of plagioclase and orthopyroxene, and mineral compositions range from ~An_{41-55} for plagioclase, En_{35-59} for orthopyroxene and En_{27-39} for clinopyroxene (Voordouw 2006).

DISCUSSION

The Hosenbein pluton shows many of the key structural, textural, and compositional characteristics of massif-type anorthosite, including (1) predominance of rocks containing 67.5–100 vol% plagioclase, (2) minor amounts of gabbronorite and ferrodiorite, (3) lack of complementary mafic–ultramafic cumulates, (4) predominantly massive adcumulate–mesocumulate texture, (5) mottling, foliation, and modal layering, (6) block structure, (7) plagioclase (An_{41-60}) and orthopyroxene (En_{28-62}) of intermediate composition, and (8) positive whole-rock Eu and Sr anomalies. As such, the following discussion on parental magmas and magmatic processes may be relevant to massif-type anorthosite in general.

Parental Magmas: Crystal to Melt Ratio and Rheology

Parental magmas for massif-type anorthosite comprise plagioclase-phyric basaltic magmas that were separated from complementary mafic–ultramafic cumulates in the crust-mantle boundary zone (Fig. 1) (Duchesne 1984; Ashwal 1993; Emslie *et al*. 1994). The composition and crystal to melt ratio of such parental magmas can be estimated from the bulk composition of the Hosenbein pluton, assuming most magma crystallized within the boundaries of the pluton. In this specific case, the estimate is reliable because the plan view and complete vertical section of the pluton are so well exposed. The weighted average for each rock type in the pluton is ~60 vol% leucogabbronorite–leuconorite, ~34 vol% anorthosite and ~6 vol% gabbronorite–ferrodiorite. Assuming mean plagioclase abundances of 80, 95 and 50 vol% for each lithology, respectively, the resultant bulk composition of the pluton is ~83 vol% plagioclase and ~17 vol% pyroxene plus accessory minerals. Further assuming that cotectic ratios of plagioclase to pyroxene equal ~7:3 (Morse, pers. comm. 2007), it follows that the parental magma to the pluton had a crystal to melt ratio around ~45:55.

The high crystal to melt ratio for magmas parental to the Hosenbein pluton and other massif-type anorthosite (e.g., Longhi *et al*. 1993) differs from the cotectic basaltic magmas inferred to be parental to Archaean megacrystic, layered intrusive, ocean basin, and lunar anorthosite. Because increasing crystal contents cause significant increases in magma viscosity (Marsh 1981; Longhi *et al*. 1993; Philpotts and Carroll 1996), it is likely that the crystallization processes of massif-type anorthosite were different as well. Yet much of the work published on Nain anorthosite describes evidence for crystallization in dynamic magmatic environments (e.g., Morse 1969a, 1972; Berg 1972, 1973; Davies 1973; Ranson 1975, 1981) that are atypical of viscous crystal-laden magma. In contrast, processes important in the crystallization of such magmas, like porous flow and cumulate compaction for example (Philpotts *et al*. 1996; Meurer and Boudreau 1998a, 1998b), are rarely invoked. The remainder of this discussion explores whether the apparent disregard of high viscosity magmatic process is consistent with textures and structures observed in the Hosenbein pluton.

Before continuing, however, it is worth briefly discussing the possible origins of Hosenbein gabbronorite–ferrodiorite, which likely crystallized from magmas with relatively low crystal to melt ratios. Possible origins for these crystal-poor magmas include (1) derivation from the same deep staging chamber that produced plagioclase-phyric magmas, (2) fractional crystallization of plagioclase-phyric magmas at the emplacement level, and (3) intrusion of magmas unrelated to the pluton (e.g., derived from other magma chambers, partial melting of mafic–ultramafic sources). In the first case, some of the basaltic melt residing in deep staging chambers may have been removed without being enriched in plagioclase phenocrysts. Such an origin is consistent with the broadly similar mineralogy of gabbronorite–ferrodiorite to that of the plagioclase cumulates, and their broadly comagmatic origin as suggested by gradational contact morphologies. The second case is most relevant to ferrodiorite, which has compositional features (sodic plagioclase, Fe-rich pyroxene, high wt% Fe-Ti-P-HFSE-REE) consistent with a residual origin (see also Mitchell *et al*. 1996; Bhattacharya *et al*. 1998). The third case is also possible but implies the remarkable coincidence that melts of appropriately similar and, in some cases, evolved compositions were selectively emplaced into the pluton during and shortly after its emplacement.

Magmatic Processes

Processes that may have been significant during crystallization of plagioclase-phyric magma in the Hosenbein pluton include (in approximate order of increasing magma viscosity) (1) convective flow, (2) crystal settling and/or flotation, (3) development of cumulate crystal frameworks, (4) porous flow of intercumulus melt, (5) compaction, and (6) synplutonic deformation. Additional processes like liquid immiscibility and deuteric alteration probably played only a minor role in crystallization, and are therefore omitted.

Convective flow

Convective flow is characteristic of low-viscosity, phenocrysts-poor, magmas like those parental to Archaean megacrystic and layered intrusive anorthosite. Igneous structures sometimes interpreted as palaeo-convective indicators include cross-beds, trough structures, foliation, and autoliths (e.g., Wager *et al*. 1960; Irvine *et al*. 1998), of which only the latter two occur in the Hosenbein pluton.

Foliation indicative of palaeo-convective flow is typically

defined by the alignment of phenocrysts, with long axes parallel to the flow direction (e.g., Paterson *et al*. 1989). In contrast, foliation within most of the Hosenbein pluton (i.e., Main Zone) is defined by the alignment of intercumulus pyroxene. Plagioclase phenocrysts, on the other hand, are randomly oriented in even the most strongly foliated rocks, suggesting it is unlikely that foliation originated through convective flow. Alternative magmatic origins for foliation include diapiric ascent, ballooning, and compaction (e.g., Barnichon *et al*. 1999; Meurer and Boudreau 1998b). Foliation developed during diapirism and ballooning would tend to concentrate along the margins of the pluton, which contrasts with the relatively uniform occurrence of foliation throughout the Main Zone. Perhaps the most likely origin is compaction, or other types of synplutonic deformation, as this is consistent with both the uniform and intercumulus nature of the foliation. The slightly more pervasive foliation developed ~1/4 of the way up the Main Zone may have resulted from the optimum combination of (1) maximum mass of overlying cumulates (to trigger compaction) with (2) thermal insulation from country rock (which delays solidification so as to allow for compaction to occur).

Foliation in the Marginal Zone is relatively scarce and only locally defined by the alignment of plagioclase and/or pyroxene phenocrysts. If this foliation originated through convection then the steep dips of these foliations imply that convective flow was driven by subhorizontal, rather than vertical, temperature gradients. Possible alternative origins include a combination of intrusion-related flow and synplutonic deformation, which could explain foliation of phenocrysts and granular-textured aggregates, as well as the spatial association with gneissic–mylonitic layering.

Autoliths of low-density roof cumulates hosted in high-density floor cumulates may have been transported downwards by convective flow (e.g., Irvine *et al*. 1998). In the Hosenbein pluton, autoliths occur only in the Marginal Zone and field relations suggest derivation through pulsating emplacement rather than transport in convective currents. Furthermore, Unity xenoliths that form block structure in the Main Zone are concentrated directly underneath unbroken exposures of Unity anorthosite, suggesting limited movement of xenoliths and thereby a lack of convective flow.

Crystal settling/flotation

The settling and flotation of cumulus crystals is also restricted to low viscosity aphyric magmas, which would allow rapid and unimpeded vertical movements of cumulus crystals. Indicators of crystal settling/flotation include modally-graded and grain size-graded layering, of which only modal layers were observed in Hosenbein outcrops, as well as cryptic layering.

Modally graded layers are widespread within layered mafic–ultramafic intrusions (e.g., Bushveld Complex) where they may form through the settling and flotation of one or more cumulus minerals. However, research indicates that magmatic modal layers may originate through many other processes (Naslund and McBirney 1996), including, for example, diapiric ascent and synmagmatic deformation (e.g., Ameglio *et al*. 1997; Barnichon *et al*. 1999; Royse *et al*. 1999; Royse and Park 2000). In the Hosenbein pluton, modal layering is most abundant in the Marginal Zone, where it shows mostly gneissic texture that locally grades into mylonite. Furthermore, these gneissic–mylonitic modal layers are subvertically oriented and strike parallel to conduits that controlled the ascent and emplacement of magmas, suggesting that modal layers originated through synplutonic deformation in magma conduits rather than crystal settling/flotation.

Modal layering in the Main Zone is sparse and significantly subordinate to massive, mottled, and foliated rocks. Furthermore, these modal layers are defined by changes in the proportions of one cumulus phase (plagioclase) and several intercumulus minerals, and so may have originated through the redistribution of intercumulus liquid rather than crystal settling/flotation. Evidence for paleo-crystal settling/flotation is therefore at best equivocal and localized.

Cryptic layering may record paleo-crystal settling and/or flotation through gradual changes in the composition of cumulus minerals (e.g., Morse 1969b), like an upward enrichment of Na in plagioclase and/or Fe in orthopyroxene. In the Hosenbein pluton, plagioclase is the only cumulus phase and shows no systematic vertical change in composition across the Main Zone. The wider range in cumulus plagioclase compositions in the Marginal Zone is likely related to the interplay of (1) pulsating emplacement of gabbronorite–ferrodiorite magmas with slightly different plagioclase compositions, (2) localized fractional crystallization of these magma pulses, and/or (3) migration of ferrodiorite residual melts from Main to Marginal Zone.

Development of plagioclase crystal frameworks

Cumulus plagioclase crystals suspended in silicate melt tend to link together and, eventually, coagulate into cumulus crystal frameworks, possibly starting at crystal to melt ratios of ~35:65 (Philpotts and Carroll 1996; Philpotts *et al*. 1996). Establishment of these frameworks results in a rapid increase in magma viscosity and the related inhibition of low viscosity magmatic processes (Philpotts and Carroll 1996).

The Main Zone contains ~85 vol% plagioclase, with most cumulus plagioclase crystals impeding on at least one neighbouring crystal. From this simple observation alone it seems almost certain that vast frameworks of cumulus plagioclase spanned across much, if not the entire, Main Zone. Furthermore, the estimated ~45:55 crystal to melt ratio of the parental magma lies well above the ~35:65 ratio required to form rigid crystal frameworks, suggesting that plagioclase crystal frameworks formed shortly after magma emplacement. Crystallization of the Main Zone may therefore have occurred exclusively

through processes typical of high viscosity magmas, consistent with the previously discussed scarcity of palaeo-convective, -crystal settling and -crystal flotation indicators.

The bulk composition of the Marginal Zone (~74% plagioclase and ~26% pyroxene plus accessory minerals) suggests that the crystal to melt ratio of parental magma was only ~15:85, well below the ~35:65 threshold for developing crystal frameworks. Hence, these magmas could have produced dynamic textures and structures for some time after emplacement. However, the significant abundance of plagioclase cumulates in the Marginal Zone (~73 vol%) suggests that the development of cumulus frameworks was inevitable and would have eventually connected frameworks in the Main Zone to the walls of the pluton. Such pluton-wide crystal frameworks play an important role in the promotion of synmagmatic deformation (Barros *et al*. 2001), as discussed further below.

Porous flow of intercumulus melt

Cumulus crystal frameworks contain intercumulus melts that are significantly more mobile than the cumulus phases (McBirney and Hunter 1995; Philpotts and Carroll 1996; Philpotts *et al*. 1996). These melts can crystallize *in situ* to form intercumulus minerals or they can be aggregated through porous flow and, in places, segregated (e.g., Philpotts *et al*. 1996; Mitchell *et al*. 1996; Bhattacharya *et al*. 1998). In the Hosenbein pluton, possible textural and structural indicators for the palaeo-porous flow of intercumulus melts include (1) mottled texture (2) pyroxenite aggregates, and (3) ferrodiorite dykes and patches. As discussed previously, the composition and gradational contacts of ferrodiorite bodies are consistent with an origin through the aggregation and segregation of residual melts (Mitchell *et al*. 1996; Bhattacharya *et al*. 1998).

Mottled rocks can be interpreted as plagioclase cumulate that crystallized with heterogeneously distributed intercumulus melt, as a homogeneous distribution would have produced a massive rock. Perhaps this heterogeneous distribution was the result of low nucleation rates at a late stage in the crystallization process, which forced dissolved pyroxene components to move towards existing intercumulus nuclei rather than nucleating *in situ*. In this case, these components would have used porous flow to move towards nucleation sites. There are few other viable interpretations for mottled texture. A cotectic cumulate origin, for example, is inconsistent with the lack of optical continuity of orthopyroxene in individual patches and the lack of crystal-settling structures.

Pyroxenite aggregates may also have originated from a combination of porous flow and low nucleation rates, which would have facilitated concentration of pyroxene components and the growth of large crystals. Vein-like aggregates may have formed in planar zones of high porosity developed during late-magmatic fracturing of the cumulus plagioclase framework, possibly in response to cooling (Petersen 1987), tectonic stresses (Barros *et al*. 2001), and/or compaction (Philpotts *et al*. 1996). Pod-like aggregates may have formed in a similar way but had room to grow in three, rather than just two, dimensions. Corona-type aggregates that formed on xenolith margins may be analogous to pegmatoidal "strain shadows" reported in some granitoids, which formed through the flow of intercumulus melt into low-pressure areas generated by the rotation of xenoliths during late-magmatic deformation (Paterson and Miller 1998).

Compaction

Compaction causes the densification of cumulates and simultaneous removal of intercumulus melt through porous flow (Hunter 1996). Textural and structural indicators of compaction include adcumulate texture (Hunter 1996) and high-T deformation microstructures (Lafrance *et al*. 1996). Possible driving forces include the weight of overlying cumulates (McKenzie 1984) and synplutonic stress (Barros *et al*. 2001), the latter of which is especially effective if the pluton is traversed by crystal frameworks (Barros *et al*. 2001).

Adcumulate textures may evolve through compaction (Hunter 1996) or efficient chemical exchange between intercumulus liquid and a continuously convecting, overlying, melt reservoir (Tait *et al*. 1984; Morse 1986). Within Main Zone anorthosite, adcumulate textures are widely developed and associated with low abundances of intercumulus minerals. The origin of these adcumulate textures through exchange with an overlying reservoir would be indicated by preservation of either significant plagioclase-pyroxene rocks with cotectic proportions and/or complementary mafic–ultramafic cumulates. Neither is significantly developed within the Hosenbein pluton. In contrast, the widespread evidence for palaeo-porous flow and, as discussed below, high-T deformation structures, suggest that an origin through compaction is more tenable.

The high-T deformation microstructures that are so widely developed in the Main Zone likely formed during crystallization, as the Nain batholith cooled and was uplifted almost immediately after its emplacement (Hill 1982; Wiebe 1985). In this case, possible origins for these microstructures include compaction and diapiric ascent. The latter is unlikely since the pluton lacks the diapiric intrusive form as characterized in previous works (Wiebe 1992; Barnichon *et al*. 1999). Compaction, on the other hand, is consistent with the widespread development of adcumulate texture and the indicators for paleo-porous flow of intercumulus melt. More specifically, compaction driven by synmagmatic tectonics is consistent with conduit-parallel gneissic–mylonitic layering within the Marginal Zone as well as the inferred development of trans-pluton crystal frameworks. Compaction driven by the weight of overlying cumulates, on the other hand, is unlikely because the cumulus minerals had similar to lower density relative to the intercumulus melt.

Two other features in the Main Zone may be consistent with compaction; (1) the lower half contains a higher proportion of anorthosite than the upper half, and (2) gabbronorite–ferrodiorite dykes in the lower half tend to be thinner than those in

the upper half. Collectively, these features suggest that intercumulus melts moved upwards from the lower half of the Main Zone into the upper half and, possibly, the Upper Marginal Zone (possibly explaining the occurrence of Fe-rich pyroxene in this part of the pluton).

Synplutonic deformation

Synplutonic deformation may be related to diapirism and/or synplutonic tectonic activity, and is indicated by (1) high-T deformation microstructures within igneous minerals (Lafrance *et al*. 1996), (2) gneissic fabrics within pluton margins (e.g., Barnichon *et al*. 1999), and, in some cases, (3) foliation. Possible origins of high-T deformation and foliation through synplutonic deformation were discussed previously.

Gneissic–mylonitic fabrics are relatively abundant in the Marginal Zone of the Hosenbein pluton, where they strike parallel to crustal-scale magma conduits. Hence, these fabrics may have formed through synplutonic deformation of the Marginal Zone on magma conduits (e.g., Ameglio *et al*. 1997; Royse and Park 2000). Alternative origins include diapiric ascent and ballooning, the former being unlikely as the pluton lacks a diapir-like structure. Ballooning-related deformation, on the other hand, is typically driven by swelling as magma is emplaced into the central part of the pluton. The Marginal Zone, however, strikes parallel to conduits that were widely exploited during emplacement of the Nain batholith, suggesting that magmas were emplaced along the margins rather than in the central part of the pluton.

SUMMARY AND CONCLUSIONS

The key to determining the magmatic processes that controlled crystallization of the Hosenbein pluton is in unravelling the relative abundances of igneous textures/structures, and to find the common denominator for the most abundant features. This approach suggests that the following processes were important: (a) development of cumulus crystal frameworks, (b) porous flow of intercumulus melt, (c) compaction and (d) tectonically induced synplutonic deformation. Just as important is that these processes are consistent with the crystallization of a viscous plagioclase-phyric parental magma.

The contrast between interpretations made in this study and those in previous work illustrate how theoretical models are both developed by and guide field observations. The seminal work done on Nain anorthosite in the 1970s occurred shortly after the development of models explaining layering in the Skaergaard and Bushveld intrusions, motivating field geologists keen to test this model to search for indicator structures in other intrusive rocks. Although the Nain anorthosites do indeed contain such features, the later (1980s and 1990s) development of models suggesting alternative origins for igneous structures and petrogenetic schemes for massif anorthosite worked against interpretations that Nain anorthosite evolved in dynamic magma chambers. The results of this study also demonstrate that it is important to consider the relative abundance of igneous structures rather than the occurrence of a single cross-bedded or size-graded layer.

The Hosenbein pluton is ideally suited for future investigations of massif-type anorthosite and magmatic processes, as it is the only intrusive body directly accessible from the town of Nain. Future investigations could focus on providing geochemical and theoretical constraints on magmatic processes through, for example, testing for isotopic disequilibrium between cumulus and intercumulus phases and detailed structural analysis.

ACKNOWLEDGEMENTS

I thank my PhD supervisor, John Myers, for funding and encouraging the research. Paul Sylvester and Pam King are thanked for producing whole-rock geochemical data. Mike Schaeffer and Maggie Piranian helped with electron microprobe analyses. Fieldwork was done with the assistance of Warren Brown, Johan Voordouw, and Cory Furlong. Thanks also to Voisey's Bay Nickel Company (VBNC) for logistical support in the field. The research was funded by Natural Sciences and Engineering Research Council (NSERC) and VBNC through a CRD project grant (CRDPJ 233669-99) to John Myers. Additional funds were provided through an NSERC postgraduate fellowship, the Estate of Alfred K. Snelgrove and the School of Graduate Studies. The author thanks the journal reviewers and editor for their helpful comments that led to clarifications and improvements in the manuscript.

REFERENCES

Ameglio, L., Vigneresse, J.L., and Bouchez, J.L. 1997. Granite pluton geometry and emplacement mode inferred from combined fabric and gravity data. *In* Granite: from segregation of melt to emplacement fabrics. *Edited by* J.L. Bouchez. Kluwer Academic Press, Dordrecht, pp. 199–214.

Ashwal, L. D. 1993. Anorthosites. Springer-Verlag, Berlin, 422 p.

Ashwal, L.D., Morrison, D.A., Phinney, W.C., and Wood, J. 1983. Origin of Archean anorthosites: evidence from the Bad Vermillion Lake complex, Ontario. Contributions to Mineralogy and Petrology, 82, pp. 259–273. doi:10.1007/BF01166620

Barnichon, J.D., Havenith, H., Hoffer, B., Charlier, R., Jongmans, D., and Duchesne, J.C. 1999. The deformation of the Egersund-Ogna anorthosite massif, south Norway: finite-element modeling of diapirism. Tectonophysics, 303, pp. 109–130. doi:10.1016/S0040-1951(98)00247-9

Barros, C.E.M., Barbey, P., and Boullier, A.M. 2001. Role of magma pressure, tectonic stress and crystallization prog-

ress in the emplacement of syntectonic granites. The A-type Estrela granite complex (Carajas Mineral Province, Brazil). Tectonophysics, 343, pp. 93–109. doi:10.1016/S0040-1951(01)00260-8

Berg, J.H. 1972. Geology of the Hettasch Lake area. *In* Nain Anorthosite Project field report. *Edited by* S.A. Morse. University of Massachusetts, pp. 49–64.

Berg, J.H. 1973. Further study of the Hettasch intrusion and associated rocks. *In* Nain Anorthosite Project field report. *Edited by* S.A. Morse. University of Massachusetts, pp. 107–119.

Bhattacharya, A., Raith, M., Hoernes, S., and Banerjee, D. 1998. Geochemical evolution of the massif-type anorthosite complex at Bolangir in the Eastern Ghats belt of India. Journal of Petrology, 39, pp. 1169–1193. doi:10.1093/petrology/39.6.1169

Davies, H.M. 1973. Emplacement sequence of anorthositic rocks in the southeastern portion of the Nain Complex. *In* Nain Anorthosite Project field report. *Edited by* S.A. Morse. University of Massachusetts, pp. 59–66.

de Waard, D., Mulhern, K., and Merriam, D.F. 1976. Mineral variation in anorthositic, troctolitic, and adamellitic rocks of the Barth Island Layered Structure in the Nain Anorthosite Complex, Labrador. Mathematical Geology, 8, pp. 561–574. doi:10.1007/BF01042994

Duchesne, J.C. 1984. Massif anorthosites: another partisan review. *In* Feldspar and Feldspathoids, NATO ASI. *Edited by* W.L. Brown. Kluwer Academic Press, Dordrecht, pp. 411–433.

Eales, H.V., Marsh, J.S., Mitchell, A.A., de Klerk, W.J., Kruger, F.J., and Field, M. 1986. Some geochemical constraints upon models for the crystallization of the upper critical zone-main zone interval, northwestern Bushveld complex. Mineralogical Magazine, 50, pp. 567–582. doi:10.1180/minmag.1986.050.358.03

Emslie, R. F., Hamilton, M. A., and Thériault, R. J. 1994. Petrogenesis of a Mid-Proterozoic anorthosite-mangerite-charnockite-granite (AMCG) complex: isotopic and chemical evidence from the Nain Plutonic Suite. Journal of Geology, 102, pp. 539–558. doi:10.1086/629697

Emslie, R.F., and Stirling, J.A.R. 1993. Rapakivi and related granitoids of the Nain Plutonic Suite: Geochemistry, mineral assemblages, and fluid equilibria. Canadian Mineralogist, 31, pp. 821–847.

Evans-Lamswood, D.M., Butt, D.P., Jackson, R.S., Lee, D.V., Muggridge, M.G., Wheeler, R.I., and Wilton, D.H.C. 2000. Physical controls associated with the distribution of sulfides in the Voisey's Bay Ni-Cu-Co deposit, Labrador. Economic Geology, 95, pp. 749–769. doi:10.2113/95.4.749

Funck, T., Louden, K.E., and Reid, I.D. 2000. Wide-angle seismic imaging of a Mesoproterozoic anorthosite complex: The Nain Plutonic Suite in Labrador, Canada. Journal of Geophysical Research, 105, pp. 25693–25707. doi:10.1029/2000JB900237

Gaskill, O.D. 2005. Geology of the 1.33 – 1.32 Ga Barth Island Ring Complex, near Nain, Labrador. Unpublished M.Sc. thesis, Memorial University of Newfoundland, St John's, Canada, 257 p.

Haskin, L.A., Haskin, M.A., Frey, F.A., and Wildman, T.R. 1968. Relative and absolute abundances of the rare earths. *In* Origin and distribution of the elements, vol. 1. *Edited by* L.H. Ahren. Pergamon, Oxford, pp. 889–911.

Hill, J.D. 1982. Geology of the Flowers River-Notakwanon River area, Labrador. Newfoundland Department of Mines and Energy, Report 82-6, 140 p.

Hunter, R.H. 1996. Texture development in cumulate rocks. *In* Layered Intrusions. *Edited by* R.G. Cawthorne. Elsevier, Amsterdam, pp. 77–101.

Irvine, T.N., Anderson, J.C.Ø, and Brooks, C.K. 1998. Included blocks (and blocks within blocks) in the Skærgaard intrusion: Geologic relations and the origins of rhythmic modally graded layers. Geological Society of America Bulletin, 110, pp. 1398–1447. doi:10.1130/0016-7606(1998)110<1398:IBABWB>2.3.CO;2

Kruger, F.J., and Marsh, J.S. 1985. The mineralogy, petrology and origin of the Merensky cyclic unit of the Bushveld Complex. Economic Geology, 80, pp. 958–974. doi:10.2113/gsecongeo.80.4.958

Lafrance, B., John, B.E., and Scoates, J.S. 1996. Syn-emplacement recrystallization and deformation microstructures in the Poe Mountain anorthosite, Wyoming. Contributions to Mineralogy and Petrology, 122, pp. 431–440. doi:10.1007/s004100050139

Longerich, H.P., Jenner, G.A., Fryer, B.J., and Jackson, S.E. 1990. Inductively Coupled plasma-mass spectrometric analysis of geological samples; a critical evaluation based on case studies. Chemical Geology, 83, pp. 105–118. doi:10.1016/0009-2541(90)90143-U

Longerich, H. 1995. Analysis of Pressed Pellets of Geological Samples using Wavelength-Dispersive X-Ray Fluorescence Spectrometry. X-Ray Spectrometry, 24, pp. 123–126. doi:10.1002/xrs.1300240309

Longhi, J. 1978. Pyroxene stability and the composition of the lunar magma ocean. *In* Proceedings of the 9thLunar Planetary Science Conference. Geochimica et Cosmochimia Acta supplement 11, pp. 285–306.

Longhi, J., Fram, M.S., Vander Auwera, J., and Montieth, J.N. 1993. Pressure effects, kinetics, and rheology of anorthositic and related magmas. The American Mineralogist, 78, pp. 1016–1030.

Marsh, B.D. 1981. On the crystallinity, probability of occurrence and rheology of lava and magma. Contributions to Mineralogy and Petrology, 78, pp. 85–98. doi:10.1007/BF00371146

McBirney, A.R., and Hunter, R.H. 1995. The cumulate paradigm reconsidered. The Journal of Geology, 103, pp. 114–122. doi:10.1086/629727

McKenzie, D. 1984. The generation and compaction of partially molten rock. Journal of Petrology, 25, pp. 713–765.

Meurer, W.P., and Boudreau, A.E. 1998a. Compaction of ig-

neous cumulates part I: geochemical consequences for cumulates and liquid fractionation trends. The Journal of Geology, 106, pp. 281–292. doi:10.1086/516022

Meurer, W.P., and Boudreau, A.E. 1998b. Compaction of igneous cumulates part II: compaction and the development of igneous foliations. The Journal of Geology, 106, pp. 293–304. doi:10.1086/516023

Mitchell, J.N., Scoates, J.S., Frost, C.D., and Kolker, A. 1996. The geochemical evolution of anorthosite residual magmas in the Laramie anorthosite complex, Wyoming. Journal of Petrology, 37, pp. 637–660. doi:10.1093/petrology/37.3.637

Morse, S.A. 1969a. Layered intrusions and anorthosite genesis. *In* Origin of anorthosite and related rocks. *Edited by* Y.W. Isachsan. New York State Museum Science Service, Memoir 18, Albany, pp. 175–187.

Morse, S.A. 1969b. The Kiglapait layered intrusion, Labrador. Geological Society of America, Memoir 112, 204 p.

Morse, S.A. 1972. The feldspar/magma density paradox and evidence of crystal settling: layering, lamination, channel scouring. *In* Nain Anorthosite Project field report. *Edited by* S.A. Morse. University of Massachusetts, pp. 113–116.

Morse, S.A. 1986. Convection in aid of adcumulus growth. Journal of Petrology, 27, pp. 1183–1214.

Myers, J.S., Voordouw, R.J., and Tettelaar, T. 2008. Proterozoic anorthosite-granite Nain batholith: structure and intrusion processes in an active lithosphere-scale fault zone, northern Labrador. Canadian Journal of Earth Science, 45, pp. 909–934. doi:10.1139/E08-041

Nakamura, N. 1974. Determination of REE, Ba, Fe, Mg, Na, and K in carbonaceous and ordinary chondrites. Geochimica et Cosmochimica Acta, 38, pp. 757–775. doi:10.1016/0016-7037(74)90149-5

Naslund, H.R., and McBirney, A.R. 1996. Mechanisms of formation of igneous layering. *In* Layered Intrusions. *Edited by* R.G. Cawthorne. Elsevier, Amsterdam, pp. 1–43.

Paterson, S.R., and Miller, R.B. 1998. Stoped blocks in plutons: paleoplumb bobs, viscometers, or chronometers? Journal of Structural Geology, 20, pp. 1261–1272. doi:10.1016/S0191-8141(98)00066-2

Paterson, S.R., Vernon, R.H., and Tobisch, O.T. 1989. A review of criteria for the identification of magmatic and tectonic foliations in granitoids. Journal of Structural Geology, 11, pp. 349–363. doi:10.1016/0191-8141(89)90074-6

Petersen, J.S. 1987. Solidification contraction: another approach to cumulus processes and the origin of igneous layering. *In* Origins of Igneous Layering. *Edited by* I. Parsons. D. Reidel Publishing Co., Dordrecht, pp. 505–526.

Philpotts, A.R., and Carroll, M. 1996. Physical properties of partly melted tholeiitic basalt. Geology, 24, pp. 1029–1032. doi:10.1130/0091-7613(1996)024<1029:PPOPMT>2.3.CO;2

Philpotts, A.R., Carroll, M., and Hill, J.M. 1996. Crystal-mush compaction and the origin of pegmatitic segregation sheets in a thick flood-basalt flow in the Mesozoic Hartford basin, Connecticut. Journal of Petrology, 37, pp. 811–836. doi:10.1093/petrology/37.4.811

Ranson, W.A. 1975. Geology of the Iglokhsoakhtaliksoakh Lake area. *In* Nain Anorthosite Project field report. *Edited by* S.A. Morse. University of Massachusetts, pp. 35–50.

Ranson, W.A. 1981. Anorthosites of diverse magma types in the Puttuaaluk Lake area. Nain complex, Labrador. Canadian Journal of Earth Sciences, 18, pp. 26–41.

Royce, K.R., Noble, S.R., Tarney, J., and Cadman, A.C. 1999. Country-rock contamination of marginal mafic granulites bordering the Nain Plutonic Suite: implications for mobilization of Sr during high-grade contact metamorphism. Canadian Journal of Earth Sciences, 36, pp. 985–997. doi:10.1139/cjes-36-6-985

Royce, K.R., and Park, R.G. 2000. Emplacement of the Nain Anorthosite: diapiric versus conduit ascent. Canadian Journal of Earth Sciences, 37, pp. 1195–1207. doi:10.1139/cjes-37-8-1195

Rubins, C.C., and de Waard, D. 1971. Granulite zones in anorthosite near Nain, Labrador. Akademie van Wettenschappen, Amsterdam, Series BB, 74, pp. 263–268.

Rubins, C.C. 1973. Structural, stratigraphic and petrological relations of rocks south of the Barth Island intrusion, Labrador. Unpublished PhD thesis, University of Vermont, Burlington, Vermont, 100 p.

Ryan, B. 2000. Geological investigations in the type locality of the Nain Plutonic Suite (NTS 14C/12). *In* Current Research Geological Survey Report 2000-1. Newfoundland Department of Mines and Energy, pp. 251–277.

Ryan, B. 2001. A provisional subdivision of the Nain Plutonic Suite in its type-area, Nain, Labrador (NTS Map Area 14C/12). *In* Current Research Geological Survey Report 2001-1. Newfoundland Department of Mines and Energy, pp. 127–157.

Tait, S.R., Huppert, H.E., and Sparks, R.S.J. 1984. The role of compositional convection in the formation of adcumulate rocks. Lithos, 17, pp. 139–146. doi:10.1016/0024-4937(84)90014-8

Thompson, R.N. 1982. Magmatism of the British Tertiary province. Scottish Journal of Geology, 18, pp. 49-107. doi:10.1144/sjg18010049

Voordouw, R.J. 2006. Geology of Mesoproterozoic anorthosite intrusions in the vicinity of Nain, Labrador. Unpublished PhD thesis, Memorial University of Newfoundland, St John's, Newfoundland and Labrador, 340 p.

Wager, L.R., Brown, G.M., and Wadsworth, W.J.1960. Types of igneous cumulate. Journal of Petrology, 1, pp. 73–85.

Walker, D. 1983. Lunar and terrestrial crust formation. *In* Proceedings of the 14th Lunar Planetary Science Conference, Part I. Journal of Geophysical Research supplement 88, pp. B17–B25.

Wheeler, E.P. 1960. Anorthosite-adamellite complex of Nain, Labrador. Bulletin of the Geological Society of America, 71, pp. 1765–1782. doi:10.1130/0016-7606(1960)71[1755:ACONL]2.0.CO;2

Wiebe, R.A. 1985. Proterozoic basalt dykes in the Nain anorthosite complex, Labrador. Canadian Journal of Earth Sciences, 22, pp. 1149–1157.

Wiebe, R.A. 1992. Proterozoic anorthosite complexes. *In* Proterozoic Crustal Evolution. *Edited by* K.C. Condie. Elsevier, Amsterdam, pp. 215–261. doi:10.1016/S0166-2635(08)70120-8

Windley, B.F., Herd, R.K., and Bowden, A.A. 1973. The Fiskenæsset complex, west Greenland, Part I. A preliminary study of the stratigraphy, petrology and whole rock geochemistry from Qeqertarssuatsiaq. Geological Survey of Greenland, 106, 80 p.

Editorial responsibility: Sandra M. Barr

